Comparison of Different Experimental Techniques for the Measurement of Crystal Growth Kinetics

ARTICLE *in* CRYSTAL GROWTH & DESIGN · DECEMBER 2008

Impact Factor: 4.89 · DOI: 10.1021/cg800782r

6 AUTHORS, INCLUDING:

Alexander E.S. Van Driessche
Vrije Universiteit Brussel
44 PUBLICATIONS **348** CITATIONS
SEE PROFILE

Gen Sazaki
Hokkaido University
166 PUBLICATIONS **2,440** CITATIONS
SEE PROFILE

Mike Sleutel
Vrije Universiteit Brussel
30 PUBLICATIONS **205** CITATIONS
SEE PROFILE

Jose A. Gavira
Spanish National Research Council
97 PUBLICATIONS **1,209** CITATIONS
SEE PROFILE

Article

Comparison of Different Experimental Techniques for the Measurement of Crystal Growth Kinetics

Alexander E. S. Van Driessche, Fermi#n Ota#lora, Gen Sazaki, Mike Sleutel, K. Tsukamoto, and Jose A. Gavira

Cryst. Growth Des., **2008**, 8 (12), 4316-4323• DOI: 10.1021/cg800782r • Publication Date (Web): 11 November 2008

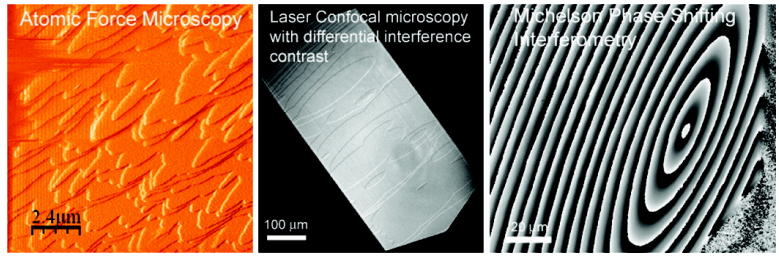

More About This Article

Additional resources and features associated with this article are available within the HTML version:

- Supporting Information
- Access to high resolution figures
- Links to articles and content related to this article
- Copyright permission to reproduce figures and/or text from this article

View the Full Text HTML

CRYSTAL GROWTH & DESIGN
2008
VOL. 8, NO. 12
4316–4323

Comparison of Different Experimental Techniques for the Measurement of Crystal Growth Kinetics†

Alexander E. S. Van Driessche,[‡] Fermín Otálora,[‡,*] Gen Sazaki,[‡,⊥,§] Mike Sleutel,[#] K. Tsukamoto,[∥] and Jose A. Gavira[‡]

Laboratorio de Estudios Cristalográficos, IACT, CSIC, Universidad de Granada, P.T. Ciencias de la Salud, Avenida del conocimiento s/n, 18100 Armilla, Granada, Spain, Institute for Materials Research, Tohoku University, Katahira, Aoba-ku, Sendai 980-8577, Japan, Ultrastructure, Flanders Interuniversity Institute for Biotechnology (VIB), Vrije Universiteit, Brussel, Belgium, and Graduate School of Science, Tohoku University, Aza-Aoba, Aramaki, Sendai 980-8578, Japan

Received July 19, 2008; Revised Manuscript Received October 30, 2008

ABSTRACT: The relative merits and domains of application of three observation techniques (atomic force microscopy, Michelson interferometry, and laser confocal microscopy with differential interference contrast microscopy) for the investigation of crystal growth kinetics are discussed in the context of protein crystallization. Growth rate measurements on the same system under identical experimental conditions using different techniques show differences up to 5-fold in growth rate and a different behavior of growth rate as a function of supersaturation. These results are discussed in terms of differences in mass transport at the crystal interface during data collection in the first case and as data processing artifacts in the second. Guidelines are provided for the selection of the optimal observation technique in crystal growth studies as a function of the specific problem under investigation, showing that AFM is best suited for nanometere-size, slow processes; LCM-DIM for nanometer−micrometer size, slow and medium processes; and PSMI for micrometer size, fast processes.

1. Introduction

After more than two decades of protein crystal growth studies, the field is reaching maturity. One of the consequences of this progress is a significant shift from phenomenological, macroscopic studies to nanoscale studies on the growth mechanisms at the crystal surface. Surface morphologies and growth kinetics of protein crystals growing from aqueous solution have been studied in situ using different observation techniques such as optical microscopy,[1] atomic force microscopy[2,3] (afm) and phase shifting Michelson interferometry[4,5] (PSMI). Also, new observation techniques like laser confocal microscopy with differential interference contrast microscopy[6] (LCM-DIM) or confocal phase shift interferometry[7] are being developed nowadays to allow for the collection of more accurate data on mescoscopic processes on entire crystal surfaces. AFM[2,3] and LCM-DIM[6,8−11] can image in situ 2D islands and spiral hillocks, allowing the direct measurement of tangential step velocities. Using interferometry, it was impossible, until recently, to achieve a resolution that allows the observation of individual 2D islands or monolayer steps on spiral hillocks.[7] So far, measurements of step velocities using interferometry were performed on spiral hillocks[4,5] and step velocities were obtained indirectly from the slope of a hillock and the normal growth rate by[12]

$$R = pv \tag{1}$$

where p is the slope of the hillock, R the normal growth rate, and v the step velocity.

An appropriate choice of the observation technique is central for the collection of useful data with the frequency and length scale resolution best suited for the problem at hand. No good or bad techniques exist per se, each technique having its own advantages and limitations, but inappropriate usage of experimentally determined kinetic data can lead to biased results of limited applicability. The literature on the assessment of these potential problems is scarce. For example, the relative movement of the AFM cantilever/tip with respect to the sample during scan could disturb solute concentration distributions in the vicinity of a crystal surface affecting the growth kinetics as suggested by Land and co-workers[13] and Gliko and co-workers,[14] but the effects, if any, of this movement on growth kinetics have not yet been systematically studied. Several comparative studies exists in the literature discussing strengths and weaknesses of each observation technique for surface profile measurements,[15−19] but comparisons of experimental data on growth kinetics obtained using different techniques for the same model system under identical experimental conditions are not available. In this work we evaluate the use of the "classical" AFM and PSMI and the newly developed LCM-DIM as observation techniques for crystal growth kinetics. For doing so, step velocities on the {110} face of tetragonal crystals of model protein hen egg white lysozyme were measured in a broad supersaturation range using these three techniques. The obtained results are compared and differences are discussed, pointing out the advantages and limitations of each technique.

2. Experimental Methods

2.1. Measuring Step Velocities with LCM-DIM, AFM, and PSMI. Growing {110} faces of tetragonal crystals of the model protein Hen Egg White lysozyme were observed in situ by AFM, LCM-DIM, and PSMI. Imaging of the step advancement with AFM was done in tapping mode using a Nanoscope IIIa multimode AFM (Veeco, Santa Barbara, CA). Standard silicon nitride and oxide sharpened SPM tips (Veeco) with nominal force constants of 0.01 N/m were used. To minimize the force applied to the crystalline surface during scanning, we continually adjusted the set point voltage to the lowest level for

† Part of the special issue (Vol 8, issue 12) on the 12th International Conference on the Crystallization of Biological Macromolecules, Cancun, Mexico, May 6−9, 2008.

* Corresponding author. E-mail: fermin@lec.csic.es. Phone: 34958 181621. Fax: 34 958 181632.

‡ Universidad de Granada.

§ Present address: The Institute of Low Temperature Science, Hokkaido University, N19−W8, Sapporo 060-0819, Japan.

⊥ Tohoku University.

Vrije Universiteit.

∥ Tohoku University.

10.1021/cg800782r CCC: $40.75
Published on Web 11/11/2008

which tip-crystal contact was maintained. A peltier element was used for a suitable temperature control of the fluid cell. Temperature inside the fluid cell was monitored with a thermocouple. Temperature fluctuations were in the range of 0.1 °C.

LCM-DIM is a new, advanced optical technique used for measuring step velocities in situ.[6,10,11] Our setup is built around a confocal system (FV300, Olympus) attached to an inverted optical microscope (IX70, Olympus) with a 20× objective lens (LUCplan FLN 20x, Olympus) and equipped with a Nomarski prism introduced into the optical path and a partially coherent superluminescent diode (Amonics Ltd., model ASLD68−050-B-FA: 680 nm) to eliminate diffraction noise. The temperature of the observation cell was controlled by two peltier elements in the range of 15.0−30.0 °C. The accuracy of the temperature control was ± 0.1 °C. More details about this experimental setup can be found in previous works.[6,8−11]

A recently developed phase-shift Michelson interferometer (PSMI)[7] was used for measuring the normal growth rates and slopes of spiral hillocks. This PSMI is equipped with a noncoherent white light source (Xe-lamp, $\lambda = 532$ nm) to increase the lateral resolving power by suppressing speckle patterns. Phase images are composed from three conventional interferograms taken with phase offsets 0, $^2/_3\pi$, and $^4/_3\pi$ by shifting the reference mirror using a piezo actuator. The intensity distribution within each interference fringe is expressed by

$$I(i)_{x,y} = a_{x,y} + b_{x,y}\cos(\phi_{x,y} + \delta(i)) \tag{2}$$

where $I(i)$ is the intensity of the conventional interferogram at each phase shifting position i, a is the background and b is the amplitude of the fringe wavelet, φ is the phase and $\delta(i)$ is the imposed phase shift, which is exactly known for each position i. When we measure $I(i)$ at offsets $\delta(i) = 0$, $^2/_3\pi$, and $^4/_3\pi$ (i.e., $i = 3$), φ as a linearized phase image can be obtained from each $I(i)$ by canceling the other independent variables

$$\phi_{x,y} = \arctan\left(\frac{\sqrt{3}(I(3)_{x,y} - I(2)_{x,y})}{2I(1)_{x,y} - I(2)_{x,y} - I(3)_{x,y}}\right) \tag{3}$$

The conversion from the contrast of the phase shift interferogram $\varphi_{x,y}$ to a height profile is done by

$$h_{x,y} = \frac{\lambda_{532}}{2\Delta n}\frac{I_{x,y}}{256} \tag{4}$$

where $h_{x,y}$ is height in nanometer at position x,y, λ is wavelength in nm, Δn is refractive index, $I_{x,y}$ is the image intensity at position x,y. With a refractive index of $\Delta n = 1.4$, a grayscale information of 8 bit corresponds to 190 nm and the theoretical resolution limit in the vertical direction is 0.74 nm. To minimize any kind of shift during the measurement, we eliminated air currents andstabilized the ambient air temperature (22.0 °C). The temperature inside the observation cell (22.0 °C) was controlled with a thermocouple and fluctuated 0.2 °C. The large working distance of the objective lenses allows for the use of sealed growth cells ensuring stable growth conditions. To improve visibility of the interference fringes, we adjusted the reflectivity of the mirror to the reflectivity of the crystal surface by inserting appropriate neutral filters. For image acquisition, a 1360 × 1024 pixel CCD camera with 8 bit grayscale resolution was used.

The observation cell ($1 \times 10 \times 20$ mm^3) used in this work for LCM-DIM and PSI observations was made out of two sandwiched glass plates of 0.17 mm thickness separated by 1 mm thick polystyrene spacers glued by silicone adhesive to one of the glass plates. After the polymerization of the adhesive, the cell was carefully washed by ultrasonic cleaning in pure (Milli-Q) water. Previously grown lysozyme seed crystals (0.1−0.3 mm in height) were transferred to the observation cell with the {110} faces parallel to the bottom glass plate. Step velocities and normal growth rates were measured at the free (upper) solution−crystal interface. For each supersaturation condition, at least two experiments with different seed crystals were carried out. At a same supersaturation, tangential rates were typically measured for a large number of steps.

For in situ AFM experiments, a seed crystal must be immobilized on a substrate which is then attached to the AFM sample holder. One commonly used method is to grow seed crystals on a rough surface (e.g., etched glass substrate,[13] electron microscopy grids[20]), but if many crystals nucleate and grow on the substrate, accurate estimation of supersaturation during AFM observations of crystal growth becomes unreliable. An alternative method is to transfer a seed crystal to the substrate of an AFM observation cell with a drop of mother liquid and clamp the crystal in place beneath flexible carbon fibers attached to the substrate.[21] For this work, a new method was designed to obtain a fixed single crystal with proper orientation, without the need of external materials such as carbon fibers. One macroseed crystal was transferred to a drop of slightly supersaturated solution on a glass substrate in a limbro plate with buffer solution containing the same concentration of precipitant as the drop. The limbro plate was sealed to prevent evaporation and incubated at 20 °C. After 24 h, the seed crystal was sufficiently attached to the glass substrate. The glass substrate was immediately mounted on the AFM holder and the fluid cell was closed to prevent evaporation. This method proved reliable and during AFM observations no movement of crystals was observed. An added advantage of this method is that crystals can be preferentially orientated.

2.2. Protein Solutions and Macroseeds. Tetragonal seed crystals of lysozyme were grown at 20.0 ± 0.1 °C from a solution containing 70 mg/ml commercial grade lysozyme (98.5%, Seikagaku), 25 mg/ml NaCl and 50 mM sodium acetate (pH 4.5) buffer. After seed crystals were transferred to the observation cell (LCM-DIM and PSMI) or glass substrate (AFM), the solution was replaced with a supersaturated solution of highly purified lysozyme ((99.99% purity, Maruwa food Inc.). Once the solution was replaced, the observation cell or glass substrate was incubated for 24 h at 20.0 °C until the surfaces of the seed crystals were completely overgrown with newly formed layers of 99.99% pure lysozyme.

2.3. Supersaturation and Solubility. To control the solubility of the protein solution, we set the observation cell on a temperature controlled stage with Peltier elements. Solubility at low temperature (15.0−26.0 °C) was calculated from solubility data reported by Sazaki and co-workers.[22] Solubility at higher temperatures (>26.0 °C) was calculated from data reported by Rosenberger and co-workers.[23]

Step velocities (v) are assumed to be a linear function of C-C_e:

$$v = \Omega\beta(C - C_e) \tag{5}$$

were $\Omega = 3 \times 10^{-20}$ cm^3 is the volume of one lysozyme molecule,[24] β is the step kinetic coefficient, C is the bulk concentration of lysozyme, and C_e the solubility. Observations were carried out in the supersaturation range $0 \leq C - C_e \leq 55$ mg/mL. This approximation, based on Chernov's hypothesis[12] on the direct integration of growth units in the steps was supported by experimental results (see Figure 2).

3. Results

Atomic force microscopy (AFM), laser confocal microscopy with differential interference contrast microscopy (LCM-DIM)m and phase shift Michelson interferometry (PSMI) were used to measure normal growth rates of {110} faces of tetragonal lysozyme crystals under identical experimental conditions. On this face, crystal growth is dominated by dislocation hillocks growth (if dislocations are present) at low and intermediate supersaturation ($C - C_e < 30$ mg/mL or $\ln(C/C_e) < 1.3$), whereas 2D nucleation mediated growth is dominant at higher supersaturations ($C - C_e > 40$ mg/mL or $\ln(C/C_e) > 1.6$), in the mid range of supersaturations both mechanisms contribute simultaneously to the growth rate. The 2D islands and spiral hillocks formed on the {110} face in a 99.99% purity solution are lens-shaped with sharp tips.[9,21] This shape results from an intrinsic anisotropy in the step velocities, being ⟨001⟩ the slow direction and ⟨110⟩ the fast direction.[2,25,26] The ratio of fast to slow directions is ∼6. [9−11,27]

Figure 1a shows a typical AFM image of a growing {110} face of a tetragonal lysozyme crystal; crystal growth proceeds by 2D nucleation at this relatively high supersaturation ($C - C_e = 54.6$ mg/mL). The lower part of the image (labeled "1D") shows a time-space image (recorded with the Y scan axis disabled so that the vertical direction encodes time, see for example the work by Kitamura and co-workers[28]). The upper part (labeled "2D") shows the XY (space-space) image obtained

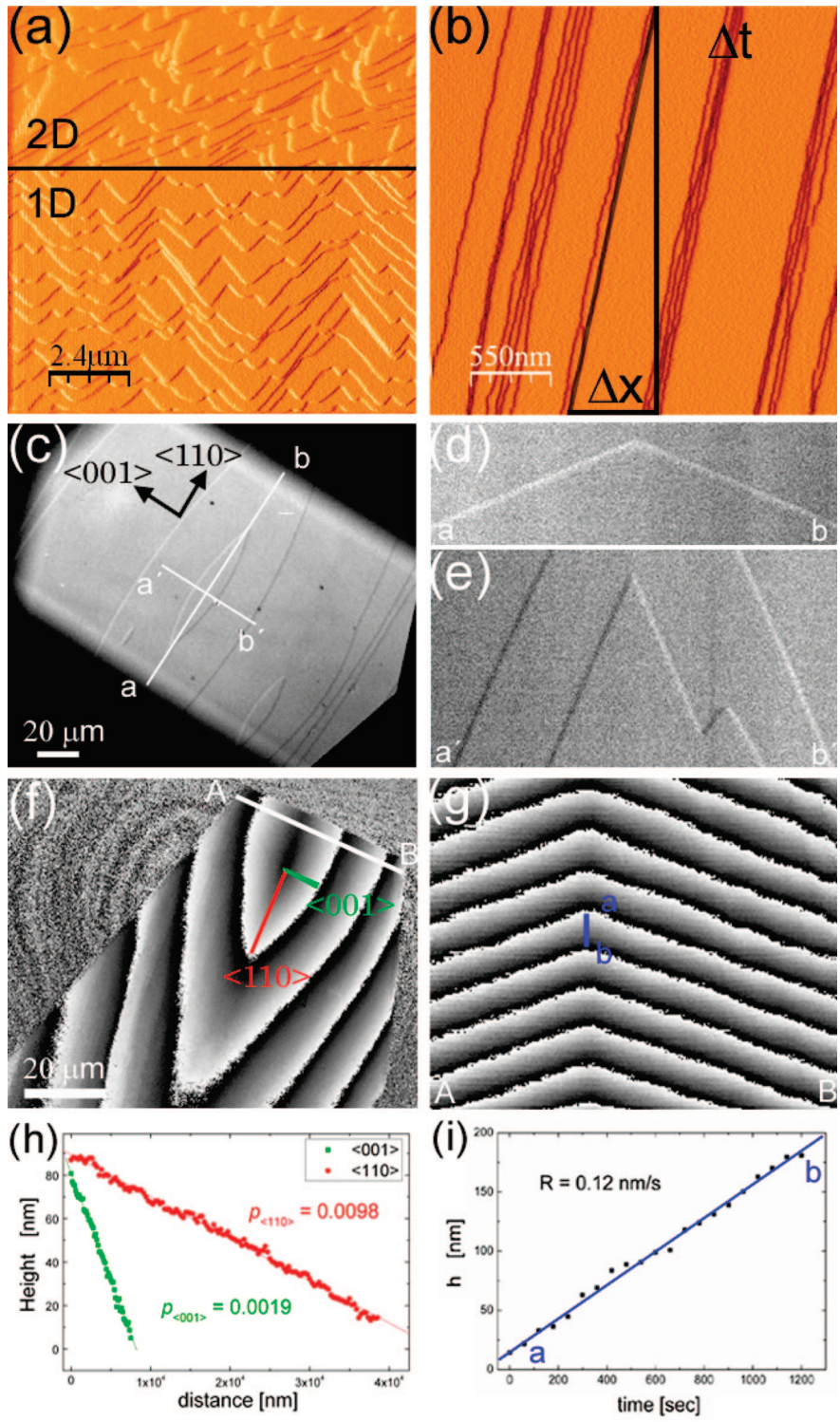

Figure 1. AFM, LCM-DIM, and PSMI images of growing {110} faces of tetragonal lysozyme crystals. (a) AFM image showing nucleation and growth of 2D islands (the horizontal line indicates transition from a time-space scan to a space-space scan). (b) Time-space AFM scan of step trains advancing at constant velocity (the Y-axis represents time). (c) LCM-DIM image of an entire {110} face showing monolayer 2D islands. (d, e) Time-space plots of step advancement in the ⟨001⟩ and ⟨110⟩ directions. (f) A typical phase shift interferogram of a spiral hillock on a {110} face. Along the line A−B, a time-space plot is constructed for the entire length of the experiment (24 h). (h) Hillock slopes in the ⟨110⟩ and ⟨001⟩ directions obtained directly from image (f). (i) The normal growth rate is directly determined from eq 4 by plotting the height at a given position on the crystal surface against its corresponding time.

when the scan in the Y direction was enabled again, depicting a high density of 2D islands that corresponds to the relatively high supersaturation at which the crystal was growing. Therefore, this picture summarizes the kind of kinetic information one can obtain from an AFM experiment: 2D nucleation density, roughness of the surface and step velocity. Figure 1b shows a time-space scan of steps on the {110} face growing at low supersaturation ($C - C_e = 6.9$ mg/mL) in the ⟨001⟩ direction. Step trains were moving at constant velocity and the interstep distance stayed constant over time. Because the scan frequency is known, step velocity can be directly determined from these time-space images provided that the scan is perpendicular to

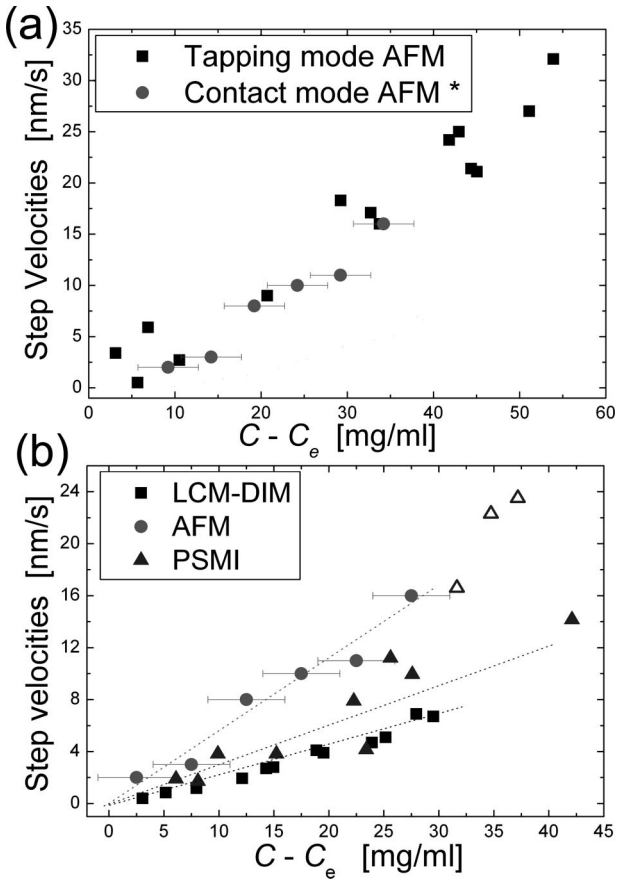

Figure 2. Step velocities measured in the ⟨001⟩ direction on {110} faces of tetragonal lysozyme crystals growing from purified lysozyme solution. (a) Comparison of step velocities measured by Tapping and contact mode AFM. (b) Comparison of step velocities obtained by AFM, LCM-DIM and PSMI. Open triangles indicate step velocities calculated from PSMI data obtained above a critical supersatersaturation ($C - C_e > 30$ mg/mL) where 2D nucleation becomes important. *Data obtained by Nakada.[31]

the step line or the angle between the step line and the scan direction is measured[29,30] by, for example, also collecting a space-space image as in the upper part of Figure 1a.

Figure 1c shows a typical LCM-DIM image of a growing {110} face. The vertical resolution of the image allows for the observation of individual steps so the same kinetic information available to AFM experiments (2D nucleation density, roughness of the surface and step velocity) can be obtained with LCM-DIM using basically the same time-space pictures for the tangential growth of specific 2D islands or dislocation hillocks (images d and e in Figure 1). These time-space pictures are constructed by extracting the pixels of a specific line in the bitmap (white lines in Figure 1c), along which the step advancement over time is observed. Each of these lines from consecutive frames will be a row in the time-space picture. Figure 1d shows one such time-space plot for the birth and spread of a 2D island ($C - C_e = 9.9$ mg/mL). The island spreads with equal velocity, $v = 8.7$ nm/s, into the positive and negative ⟨110⟩ direction. The same observations were made for the ⟨001⟩ direction having steps growing at $v = 1.4$ nm/s (Figure 1e). Step velocities were found to be constant over time.

A typical PSMI interferogram of a spiral hillock is shown in Figure 1f. From a series of these interferograms collected at regular intervals (each 60 s in this case), a time-space picture along a certain line is constructed (Figure 1g) from which the normal growth rate can be directly determined by plotting the

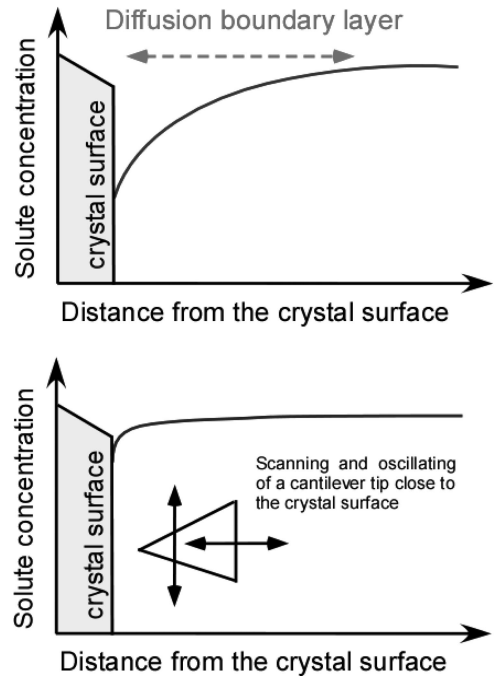

Figure 3. Schematic representation of the possible influence of the cantilever movement during in situ AFM crystal growth observations. The width of the diffusive boundary is reduced and concentration at the interface is increased by the solution stirring induced by the cantilever movement.

height at the given point (eq 4) against the corresponding time (Figure 1i). Step velocities are computed from the normal growth rate using eq 1 and the hillock slopes measured in the ⟨110⟩ and ⟨001⟩ directions on the space-space image (Figure 1h). From a time-space picture, step velocities can be directly obtained but lateral resolution is much lower than the vertical resolution and data obtained in this way will have a much larger error range.

Step velocities as a function of supersaturation measured using tapping and contact mode AFM in the ⟨001⟩ direction on {110} faces of tetragonal lysozyme are shown in Figure 2a. Contact mode AFM data are taken from Nakada[31] and were collected under identical experimental conditions. During these measurements, supersaturation was varied by changing the lysozyme concentration C and keeping constant temperature at 24 ± 1 °C. No significant difference is observed between data obtained by these two AFM operational modes. The comparison of step velocities measured as a function of supersaturation using PSMI, contact mode AFM and LCM-DIM in the ⟨001⟩ direction on {110} faces of tetragonal lysozyme are shown in Figure 2b. As could be expected from the indirect nature of the measurement, the PSMI data show the largest data scattering. Significant differences are observed between step velocities measured using different techniques: LCM-DIM data are systematically lower than AFM data. Step velocity data obtained by PSMI, at constant temperature (22.0 °C), show significant scattering but are comparable to LCM-DIM data at low superstation levels (triangles Figure 2b). For higher supersaturation levels ($C - C_e > 30$) a steep increase in the step velocities is observed from the PSMI data. From this plot, it is clear that step velocities measured by AFM (either in tapping or contact mode) are significantly faster than those measured by LCM-DIM and PSMI, and the kinetic coefficients (slope of the plot) are also larger when measured using AFM. The values for the kinetic coefficient β_{st} evaluated from the slopes of the three data sets

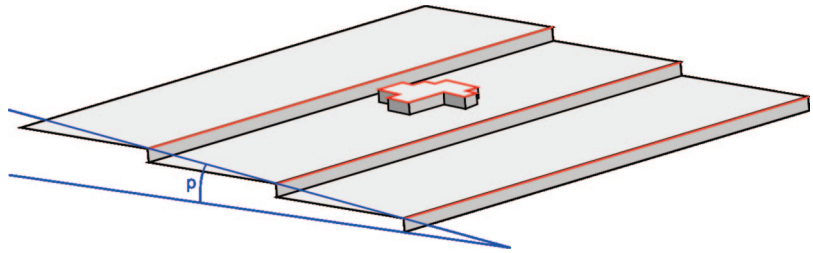

Figure 4. Schematic representation of 2D dimensional islands nucleating on the terraces of spiral hillocks. This nucleation does not significantly change the overall slope of the hillock but is important for the step density (red lines) and kink site density. Furthermore, these new 2D islands are not detectable by Michelson interferometry, which makes data analysis error prone.

in Figure 2 are 4.38×10^{-5} cm/s for AFM data, 2.64×10^{-5} cm/s for PSMI data, and 1.67×10^{-5} cm/s for LCM-DIM data. Obviously, these "technique-dependent" values for a fixed, intrinsic parameter do not have a physical meaning and are given here to provide a sense of how much the experimentally determined coefficients can change as a function of the used observation technique.

4. Discussion

4.1. Kinetic Measurements. The three techniques allow the quantification of normal and lateral growth rate, although the direct measurement of lateral growth is not possible using PSMI, which renders this technique less accuracy because of the uncertainties in the face slope p (see eq 1). Normal growth rates can be measured using AFM and LCM-DIM (if previous data about the step height are available) simply by counting the newly formed layers over time, but this is only possible for supersaturation values low enough as to avoid step overlapping at a lateral scale smaller than the microscope resolution. In both cases, the unambiguous identification of single monolayer steps is central to their use in the evaluation of kinetic data.

Step velocities measured by AFM were significantly faster than those measured by LCM-DIM. In the case of AFM, a cantilever is oscillating at a high frequency inside of the solution (tapping mode) and scanning rapidly across the surface (tapping and contact mode), close to the crystal surface. The movement of a cantilever significantly stirs the diffusion boundary layer developed in the vicinity of a growing crystal, providing a constant supply of solute molecules to the advancing steps. Consequently, the effective concentration at the step edge is increased which should result in the faster step velocities measured by AFM. Hence the most probable cause of the difference in measured step velocities is due to the cantilever movement when the crystal grows in the diffusion controlled or mixed regimes. Because data obtained from tapping mode AFM and contact mode AFM correspond well, it seems that both have a comparable effect on the mixing of the boundary layer, although, tapping mode AFM measurements show more dispersion of the data, which could be the result of the rapidly oscillating cantilever producing significant fluctuations at the step front. Effects of cantilever movement during AFM observations were also reported by Land and co-workers[13] who found that the growth rates of canavalin crystals were locally enhanced by the scan of a cantilever. Gliko and collaborators[14] argued that large variations in step velocities of lumazine synthase crystals would also be the result of the cantilever oscillation.

These differences in measured growth rates have an important impact on any quantitative calculation using the obtained kinetic data. This does not mean that one technique gives "correct data" and the other "wrong data". Different kinetic models accounting for the joint mass transport and incorporation kinetics have been proposed.[12,32,33] The assumptions and application domain of the model used for calculation must drive the selection of kinetics parameters obtained using a certain technique or the corrections needed to these parameters. The results of our work suggest that in cases where purely diffusive mass transport is assumed, parameters obtained from LCM-DIM data are best suited. In the case of data obtained with AFM it is better to assume that only surface diffusion and incorporation in the kinks are the remaining barriers for step growth because the oscillation of the cantilever originates an erratic stirring of the solution. Models based on forced convection can also be used but only in the case of laminar flow when the thickness of the boundary layer can be determined as a function of the flow velocity. When the flow velocity overcomes a critical value, the face growth will reach a steady state and grow in the kinetic regime.

Step velocities obtained from PMSI data are comparable to those directly measured by LCM-DIM at low supersaturation but for larger values ($C - C_e > 30$ or $\ln(C/C_e) > 1.3$), faster step velocities are measured using PSMI. This is, most likely, the result of significant 2D nucleation on the terraces of spiral hillocks at higher supersaturations. Because of the additional 2D nucleation the slope of the surface is no longer proportional to the step density. This proportionality is assumed in eq 1. Having more steps and kinks on a surface with roughly the same slope (Figure 4.) lead to severe overestimations of the step velocity from data on measured normal growth rates (open triangles in Figure 2b).

In general, attention must be paid to the meaning of p in eq 1. The common meaning of "p is the slope of the vicinal face" only makes sense in practice for dislocation hillocks. If 2D nucleation is present on the surface, alone or coexisting with hillocks, the more general meaning "p is the density of steps on the face" (length of steps per unit area) must be used to estimate this value. In the case of a dislocation hillock, both definitions are numerically and dimensionally equivalent. The problem of slope variations is accentuated if the slope of the hillock is measured over a short length, in which case bunched step can temporally modify the slope of the hillock. Thus temporally and/or local slope variations would explain a larger dispersions of the data points found for PSI measurements compared to AFM or LCM-DIM.

Another aspect that can make AFM an intrusive technique is the eventual occurrence of the tip/surface interactions. In contact mode AFM the interaction between cantilever and crystal takes place in the small tip−sample contact area only. Despite the low applied forces in AFM (typically nN) pressures at the tip can become so high that soft samples can be damaged. For tapping mode the physical contact with the sample is reduced to a minimum, but even so interactions are still present. In Figure 5 the effects of driving the cantilever tip into the growing surface

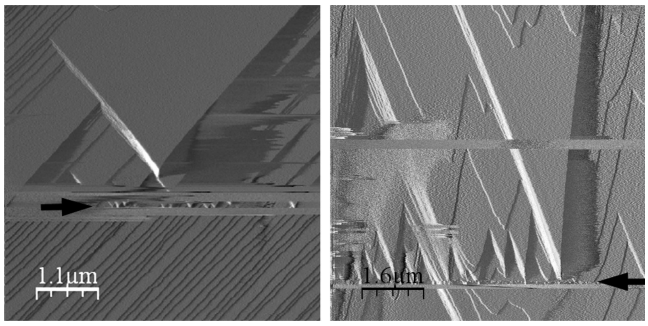

Figure 5. Effect of AFM tip interactions with the crystal surface. The black arrows indicate in each AFM images where the cantilever tip was brought into contact with the crystal surface. As a consequence 2D multilayer nucleation was provoked and the formed multilayer islands spread laterally across the surface.

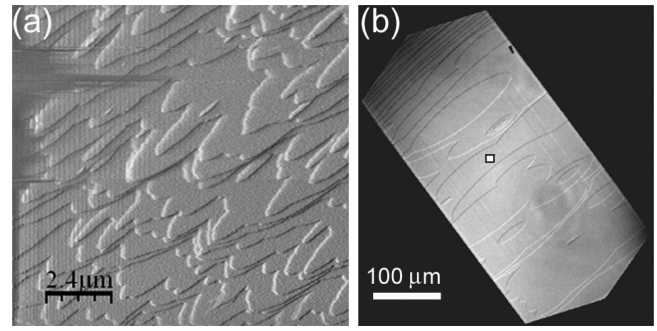

Figure 6. Comparison of the field of view observed by (a) AFM and (b) LCM-DIM. Both images show 2D islands on a {110} face of tetragonal lysozyme at (a) high supersaturation and (b) low supersaturation. The white square in image (b) represents the typical scanning size of AFM (only the significant part of the LCM-DIM image is shown).

are shown. It is quite clear that interactions of the tip with the crystal surface produced enhanced 2D nucleation. Mainly multilayer 2D islands were formed. Sharp contact of the tip with the crystal surface probably caused material to be swept from the surface and lysozyme macroclusters were created. It seems that most of these lysozyme clusters stay on the surface and give birth to multilayer 2D islands. A large plateau on top of these multilayer islands is formed as growth continues outward. Figure 5 also shows that these nuclei grow epitaxial on the crystal without, apparently, introducing defects because step trains of the multilayer islands merge flawlessly with those of the growing crystal. Tip-induced 3D macroclusters landing and consequent formation of multilayer islands was also observed for growing thaumatin[34] and canavalin crystals.[35]

4.2. Vertical, Lateral, And Time Resolutions. Unambiguous quantitative information on the surface topography is available from AFM and PSMI, but not from LCM-DIM. Therefore, additional information from the other techniques could be needed in some cases to compute normal growth rates from LCM-DIM data. The vertical resolution of LCM-DIM is around 1nm and with AFM vertical resolutions around 1 Å are possible.[3,21] Thus, both techniques have enough vertical resolution for studying single-step dynamics on protein crystals (usually nanometer step height). The theoretical vertical resolution of the PSMI's is around 1 nm (as discussed in section 2.1), but in practice, this resolution depends on the reflectivity of the crystal face, the disturbances originating at the solution or the cover glass, and the overall quality of the optical parts. Consequently, this resolution is worse for the protein surface having low reflectivity. Because of the limited resolving power of interferometry for direct observation of single steps, experimental data must be carefully evaluated to avoid biased interpretations or extrapolations beyond the resolution of the instrument. Although, recently developed, advanced PSMI techniques extend the vertical resolution to the molecular scale and are able to observe single steps at low supersaturation.[7]

Lateral resolution of PSMI and LCM-DIM is limited to that of the microscope lens used for imaging, and can be calculated using Abbe's equation (0.61λ/numerical aperture). For a $40\times$ lens, the upper limit is approximately 0.7 μm. Therefore, observation of processes below this scale requires the use of AFM. This fact is clearly seen in the space-time pictures used to evaluate the step velocity (Figure 1b, d, e). In the case of AFM, this figure shows a certain "roughness" not observed in LCM-DIM images because it exists at length scales smaller than the lateral resolution of the microscope. If you are interested in studying the kink dynamics, you will certainly choose the first, but when studying mesoscopic step dynamics (i.e., for a clean fit of the step velocity), the second is preferred.

For a fixed amount of information, the lateral resolution is the inverse of the field of view, so high lateral resolutions means small field of view. LCM-DIM and PSMI allows the observation of large areas, while AFM is more limited in lateral field of view, which can be a problem when dislocation hillocks and 2D nucleation operate simultaneously on the same surface or when the growth rate shows inhomogeneities over the crystal face. The maximum scan area for most AFMs is approximately 120 μm^2. This limitation is principally due to the operational set up of the AFM. Figure 6 shows typical AFM and LCM-DIM images of a {110} face growing by the 2D nucleation mechanism. The AFM image was scanned in 256 s and covers an area of 10×10 μm, whereas with LCM-DIM, 9.6 s were necessary to scan an area of 800×800 μm.

With interferometry, obtaining data at low supersaturation is difficult because normal growth rates are hardly detectable in the case of 2D nucleation mediated growth, while lateral (step) growth rates are larger enough to be detected. For example, 2D heterogeneous nucleation at low supersaturation has never been observed with interferometry for protein crystal growth (and seldom for small molecules),[36,37] whereas AFM studies were able to detect heterogeneous nucleation for thaumatin[20,38] and catalase[38] crystal growth. With LCM-DIM, 2D nucleation could be studied in detail for tetragonal lysozyme crystals.[9]

The high frequency domain also imposes restrictions to the acquisition of growth rate data. Typical AFM acquisition times are several minutes for large scan areas (>10 μm) and about one minute for smaller regions. In the case of in situ crystal growth observation this puts serious limitations in recording fast propagating steps. Hence, AFM remains limited to low step speeds and low supersaturation. For this reason, step velocities on {110} faces of tetragonal lysozyme could only be measured in the slow, $\langle 001 \rangle$, direction, because growth in the fast, $\langle 110 \rangle$ direction was already too fast to be followed, even at relatively low supersaturation levels.

4.3. Additional Data Quality Issues. Within their respective domains of resolution, and using adequate data processing, the three techniques show good accuracy for growth kinetics studies. The main sources of inaccuracy have been identified to be the thermal stability of the sample in the case of AFM and the mechanical stability in the case of PSMI. In the PSMI setup, the laser light is divided into two separate beams and the image quality will be more vulnerable to mechanical instability such as vibration, thermal dilation or air drag. AFM is particularly

sensitive to temperature variations because in most AFMs setup the liquid cell is directly positioned above the piezoelectric translator which is a source of heat. Astier and co-workers[31] showed that without an adequate temperature control the temperature between tip and crystal raised from 17.72 to 27.50 °C in a time period of 3 h.

Besides the possible influence on supersaturation, temperature can also modify surface kinetics or even growth mechanisms, leading to major inaccuracies in modeling and interpreting growth rate data.

5. Conclusions

Large differences (up to 5 fold increase) have been found in the measurements of growth rate, both in step velocity and kinetic coefficient, depending on the technique used. These differences are due to the presence or absence of stirring in the case of AFM and LCM-DIM respectively, because of the relative movement of the tip and the surface, and the assumptions made to convert normal growth rates into step velocities in the case of PSMI, because of the uncertainties in the value of p depending on the growth mechanism. Both situations are relevant for quantitative crystal growth research based on experimentally determined kinetic coefficients. In general, AFM data correspond better to situations were forced convection is present (i.e., no concentration gradient around the growing crystal) while LCM-DIM data, and PSMI data (after suitable correction) correspond better to diffusive mass transport situations or reduced natural convection situations (i.e., when a developed concentration depletion zone exists around the crystal).

But the selection of experimental technique is not just a matter of fitting the instrument to the mass transport and physical model relevant to the problem at hand, because the three techniques have different vertical, lateral, and time resolutions so the length and time-scales of our problem are relevant as well. PSMI shows the highest data acquisition rate but the lowest vertical and lateral resolution while AFM has the lowest acquisition rate and the highest resolution. LCM-DIM fits in between, having a vertical resolution comparable to that of AFM (at least for protein crystal growth problems), a lateral resolution like the one of PSMI, and an intermediate data acquisition rate. Therefore, AFM is the observation technique of choice for slow, nanoscale growth processes, LCM-DIM is a microscale observation technique with nanoscale vertical resolution useful for slow/medium growth processes and PSMI is the best suited technique for fast growth processes requiring only micrometric spatial resolution. Consequently, the three techniques nicely complement each other for studies on crystal growth kinetics.

In the case of protein crystal growth, the supersaturation range for which normal growth rates can be directly determined using LCM-DIM or, specially, AFM is outside the range used in most crystallization experiments for the production of crystals for X-ray diffraction. At such low growth rates, a crystal would take several months to grow to a reasonable size. AFM observations are most reliable and meaningful at low supersaturation levels where, for example, kinetics at step edges can be observed in situ. With LCM-DIM excellent observations can be carried out in the low to middle supersaturation range but at high supersaturation levels the lateral resolution is not high enough to distinguish individual steps of 2D islands. The use of interferometry is most appropriate in the middle to high supersaturation range while at low supersaturation levels macroscopic growth processes are very slow and measurements become sensible to large errors. A schematic representation of the typical operational supersaturation range for each technique is shown in Figure 7.

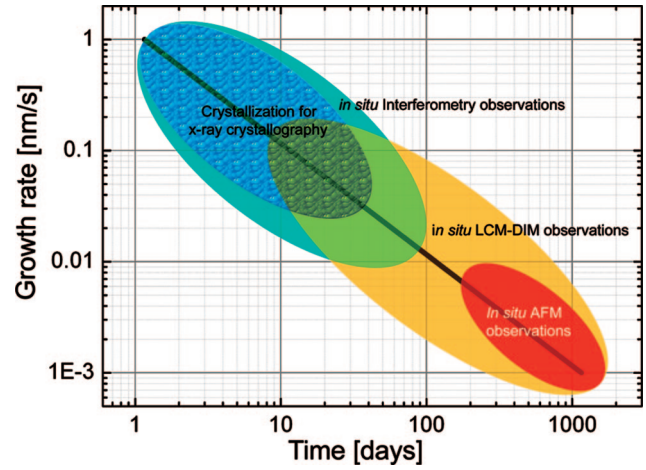

Figure 7. Typical operational supersaturation range for each technique is shown compared to the typical supersaturation ranges in which crystals for X-ray crystallography are nucleated and grown. The black line represents crystals with a size of 200 μm (modified after Dold and Tsukamoto, unpublished).

Acknowledgment. The authors thank M. Maruyama for the expertise and help in the interferometry equipment adjustment. The authors are grateful for the support by Grant ESP 2006-11327 of the Ministry of Education and Science (MEC), Spain (F.O.), the Consolider-Ingenio 2010 project "Factoría Española de cristalización", the OptiCryst project of the VII Frame Work, UE., the partial support by Grants-in-Aid (17034007 and 18360003) of Scientific Research of the Ministry of Education, Science and Culture Japan (G.S.) and Grant Intramural-200730I013 of the Consejo Superior de Investigaciones Científicas (J.A.G.).

References

(1) Pusey, M. L.; Naumann, R. *J. Cryst. Growth* **1986**, *76*, 593–599.
(2) Durbin, S. D.; Carlson, W. E. *J. Cryst. Growth* **1992**, *122*, 71–79.
(3) McPherson, A.; Kuznetsov, Y. G.; Malkin, A. J.; Plomp, M. *J. Struct. Biol.* **2003**, *142*, 32–46, and references therein.
(4) Kuznetsov, Y. G.; Malkin, A. J.; Greenwood, A.; McPherson, A. *J. Struct. Biol.* **1995**, *114*, 184–196.
(5) Gliko, O.; Booth, N. A.; Rosenbach, E.; Vekilov, P. G. *Cryst. Growth Des* **2002**, *2*, 381–385, and references therein.
(6) Sazaki, G.; Matsui, T.; Tsukamoto, K.; Usami, N.; Ujihara, T.; Fujiwara, K.; Nakajima, K. *J. Cryst. Growth* **2004**, *262*, 536–542.
(7) Tsukamoto, K.; Dold, P. In *Perspectives on Inorganic, Organic, And Biological Crystal Growth: From Fundamentals to Applications*; Skowronski, A., DeYoreo, J. J., Wang, C., Eds.; American Institute of Physics: Melville, NY, 2007; pp 329−341.
(8) Sazaki, G.; Tsukamoto, K.; Yai, S.; Okada, M.; Nakajima, K. *Cryst. Growth Des.* **2005**, *5*, 1729–1735.
(9) Van Driessche, A. E. S.; Sazaki, G.; Otálora, F.; González-Rico, F. M.; Dold, P.; Tsukamoto, K.; Nakajima, K. *Cryst Growth Des.* **2007**, *7*, 1980–1987.
(10) Van Driessche, A. E. S.; Otálora, F.; Sazaki, G.; Gavira, J. A. *Cryst Growth Des.* **2008**, *8*, 3623–3629.
(11) Van Driessche, A. E. S.; Sazaki, G.; Otálora, F.; Gavira, J. A.; Dai, G.; Matsui, T.; Yoshizaki, I.; Tsukamoto, K.; Nakajima, K. *Cryst. Growth Des.* **2008**, submitted.
(12) Chernov, A. A. *Modern Crystallography III, Crystal Growth*; Springer: Berlin, 1984.
(13) Land, T. A.; Malkin, A. J.; Kutznesov, Yu G.; McPherson, A.; De Yoreo, J. J. *J. Cryst. Growth* **1996**, *166*, 893–899.
(14) Gliko, O.; Neumaier, N.; Pan, W.; Haase, I.; Fischer, M.; Bacher, A.; Weinkauf, S.; Vekilov, P. G. *J. Am. Chem. Soc.* **2005**, *127*, 3433–3438.
(15) Komatsu, H.; Miyashita, S. *Jpn. J. Appl. Phys.* **1993**, *32*, 1478–1479.

(16) Li, J.; Li, D.; Zhang, X.; Li, X.; Zhao, A. *Proc. SPIE* **1998**, *3557*, 336–344.
(17) Lindseth, I.; Bardal, A. *Surf. Coat. Technol.* **1999**, *111*, 276–286.
(18) Conroy, M.; Armstrong, J. *J. Phys.: Conf. Ser.* **2005**, *13*, 458–465.
(19) Koyunca, I.; Brant, J.; Lüttge, A.; Wiesner, M. R. *J. Membr. Sci.* **2006**, *278*, 410–417.
(20) Malkin, A. J.; Kuznetsov, Yu. G.; Glantz, W.; McPherson, A. *J. Phys. Chem.* **1996**, *100*, 11736–11743.
(21) Malkin, A. J.; Thorne, R. E. *Methods* **2004**, *34*, 273–299.
(22) Sazaki, G.; Kurihara, K.; Nakada, T.; Miyashita, S.; Komatsu, H. J. *J. Cryst. Growth* **1996**, *169*, 355–360.
(23) Rosenberger, F.; Howard, S. B.; Sowers, J. W.; Nyce, T. A. *J. Cryst. Growth* **1993**, *129*, 1–12.
(24) Steinrauf, L. K. *Acta Crystallogr.* **1959**, *12*, 77–79.
(25) Durbin, S. D.; Feher, G. *J. Mol. Biol.* **1990**, *212*, 763–774.
(26) Li, M.; Nadarajah, A.; Pusey, M. L. *Acta Crystallogr., Sect. D* **1999**, *55*, 1036–1045.
(27) Dold, P; Ono, E.; Tsukamoto, K; Sazaki, G. *J. Cryst. Growth* **2006**, *293*, 102–109.
(28) Kitamura, N.; Lagally, M. G.; Webb, M. B. *Phys. Rev. Lett.* **1993**, *71*, 2082.
(29) Land, T. A.; DeYoreo, J. J.; Lee, J. D. *Surf. Sci.* **1997**, *384*, 136–155.
(30) Astier, J. P.; Bokern, D.; Lapena, L.; Veesler, S. *J. Cryst. Growth* **2001**, *226*, 294–302.
(31) Nakada, T. Personal communication.
(32) Burton, W. K.; Cabrera, N.; Frank, F. C. *Philos. Trans. R. Soc. London, Ser. A* **1951**, *243*, 299–358.
(33) Gilmer, G. H.; Ghez, R.; Cabrera, N. *J. Cryst. Growth* **1971**, *8*, 79–93.
(34) Kuznetsov, Y. G.; Malkin, A. J.; McPherson, A. *J. Cryst. Growth* **1999**, *196*, 489–502.
(35) Land, T. A.; DeYoreo, J. J. *J. Cryst. Growth* **2000**, *208*, 623–637.
(36) Malkin, A. J.; Chernov, A. A.; Alexeev, I. V. *J. Cryst. Growth* **1989**, *97*, 765–769.
(37) MaiwaK. TsukamotoK. SunagawaI. *Proceedings of the Fourth Topical Meeting on Crystal Growth Mechanism*; Hokkaido Press: Tokyo, 1991; pp 67−70.
(38) Malkin, A. J.; Kuznetsov, Yu. G.; McPherson, A. *J. Cryst. Growth* **1999**, *196*, 471–488.

CG800782R